Theoretical study of cubic Rashba effect at $SrTiO_3$ (001) surfaces

K. V. Shanavas*
Materials Science and Technology Division, Oak Ridge National Laboratory, Oak Ridge, Tennessee 37831-6056, USA
(Dated: November 30, 2015)

The origin of Rashba spin splitting in the two dimensional electron gas at (001) surface of $SrTiO_3$ is studied using first-principles calculations and tight-binding model. Calculations of oxygen vacancies under virtual crystal approximation reveal a 2DEG subband structure similar to polar materials, consistent with observations on $SrTiO_3$. Our studies also confirm that k dependence of the spin splitting is predominantly cubic in the surface Ti-t_{2g} states, even though structural relaxations diminish the effect in d_{xy} bands. A tight-binding model, explicitly including Ti-d and O-p states as well as next-nearest-neighbor interactions, is derived to understand the first principles results. Effective Rashba Hamiltonians for the surface bands are derived using quasi-degenerate perturbation theory and scenarios in which linear k contribution may be suppressed are discussed. However, the cubic terms in the Hamiltonian are found to be different from the model derived using $k \cdot p$ theory, leading to different pseudospin symmetry in the Brillouin zone.

I. INTRODUCTION

The perovskite oxide $SrTiO_3$ (STO), due to it's outstanding electronic properties, is an important material for the emerging field of oxide electronics[1]. It not only serves as a substrate for growing many materials, but also forms conducting interfaces with many complex oxides[2]. A highly mobile two dimensional electron gas (2DEG) forms at these interfaces,[3] which exhibit unusual properties such as superconductivity[4] and magnetism[5]. A 2DEG forms also at bare STO surfaces with a similar subband structure, possibly originating from oxygen defects[6–8]. Recently, magnetoresistance measurements on (001) surface of STO have found evidence of cubic-k Rashba splitting in the 2DEG[9].

The Rashba effect arises from an interplay between spin-orbit coupling and an inversion symmetry breaking electric field, and leads to a momentum dependent splitting of spin up and down energy bands[10]. In electron doped semiconductors[11–13] and transition metal oxides[14,15], the lowest order of Rashba splitting around zone center (Γ point) is linear in crystal momentum k. The corresponding Rashba Hamiltonian has the form $H_{\rm R1} = \alpha_{R1} i(k_-\sigma_+ - k_+\sigma_-)$, where $\sigma_\pm = 1/2(\sigma_x \pm i\sigma_y)$ are Pauli matrices, $k_\pm = k_x \pm ik_y$ denotes the crystal momentum and α_{R1} is the linear Rashba coefficient. This leads to a spin splitting of $\Delta\varepsilon_R = 2\alpha_{R1}k_{||}$ around Γ point in the surface bands.

In certain systems, such as hole doped semiconductor quantum wells, the dominant term in k is cubic[12,16–18]. This is because, holes in these systems occupy a $j = 3/2$ heavy hole band for which Rashba Hamiltonian has the form, $H_{\rm R3} = \alpha_{R3} i(k_-^3\sigma_+ - k_+^3\sigma_-)$, where α_{R3} denotes the cubic Rashba parameter. Spin-splitting grows as $\Delta\varepsilon_R = 2\alpha_{R3}k_{||}^3$ and leads to a different spin precession vector which influences SOI related phenomena[12,18]. The experimental observation of k-cubic Rashba in STO[9] is surprising because polar perovskites such as $KTaO_3$ with similar crystal structure and surface 2DEG as STO show linear splitting[14,15,19].

While cubic Rashba has been studied extensively with the help of $k \cdot p$ theory in semiconductor systems,[17] it is not well understood in d orbitals systems. Typically, theoretical models predict linear effect at polar surfaces[15,20] and interfaces[21–23]. When only coupling within t_{2g} is considered in the tight-binding model, the heavy electron band with character $d_{xz} + d_{yz}$ was found to be cubic[21,23], with strong linear splitting in other bands. In the present work, we extended the model to include full Ti-d manifold and O-p states, in order to explore the origin of cubic splitting reported by experiments. First-principles calculations on a 16.5 unitcell (uc) long TiO_2 STO slab with surface 2DEG show the splitting in Ti-t_{2g} bands to be predominantly cubic and arising from interactions between d_{xy} and d_{xz}/d_{yz} bands away from Γ point. With the help of effective Hamiltonian for the surface states, we discuss the origin of cubic splitting and the nature of pseudospins in the first Brillouin zone.

II. METHODS

The first principles calculations are carried out within density functional theory (DFT) as implemented in VASP code,[24] using projector augmented waves[25] and local density approximation. An energy cutoff of 450 eV and k space sampling on a $21 \times 21 \times 1$ grid are found sufficient to get converged results. To simulate $SrTiO_3$ (001) surface, we used a symmetric slab of $1 \times 1 \times 16.5$ unitcells with a 25 Å vacuum region to minimize interaction with periodic images. Finally, to incorporate the 2DEG at TiO_2 terminated STO surface that arise because of oxygen vacancies, we replace oxygen atoms at the surface layer partially by F within virtual crystal approximation (VCA). Since F atoms have one electron more than O, replacing surface TiO_2 with $Ti(O_{1-x}F_x)_2$ leads to $2x$ electrons per surface uc. These electrons are confined close to the surface along z, but have large dispersion in the in-plane directions. This method has been used to study electron doping effects of monolayer FeSe on STO surfaces[26]. The tight-binding models use a linear combination of atomic orbitals (LCAO) as the basis and Bloch functions to take periodicity in the x and y directions. The Hamiltonian is parametrized in terms of the Slater-Koster overlap integrals which are fit by first-principles band structures. Effective Hamiltonians for the bands around Γ point are derived based on quasi-degenerate perturbation theory as described in Ref. 27.

III. RESULTS

In the case of $LaAlO_3/SrTiO_3$ interface, alternating charges in $(LaO)^+$ and $(AlO_2)^-$ layers lead to a diverging potential inside the material, known as the polar catastrophe, which plays an important role in the formation of the electron gas[15,28]. The bare $SrTiO_3$ (001) surface, on the other hand, is made of neutral layers (of $Sr^{2+}O^{2-}$ and $Ti^{4+}O_2^{4-}$) and the 2DEG originates from oxygen vacancies that develop naturally at the surface[8] or induced by ultraviolet irradiation[6]. Two electrons per oxygen vacancy are left behind in the dangling bonds of adjacent ions. In the calculations, we used VCA to replace 20% oxygen in the surface layer by flourine, resulting in a 2DEG density of

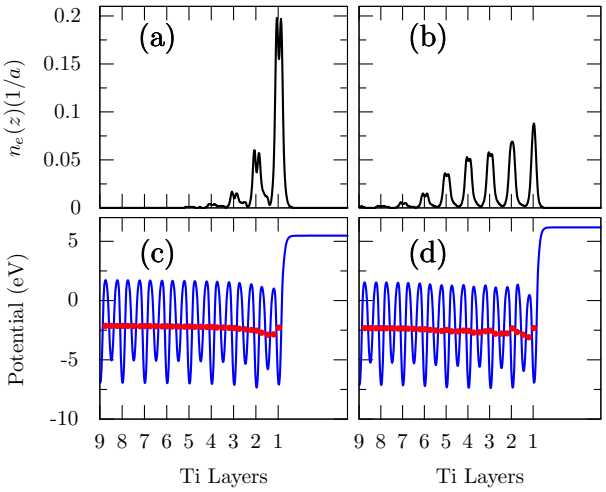

FIG. 1. (Color online) First principles calculated layer density profile at the top surface of the (a) unrelaxed and (b) relaxed TiO_2 terminated $SrTiO_3$ slab. Bottom panels show the local potential (blue curves) and layer averaged potential (red) for the two cases.

2×10^{14} cm^{-2} at the surface layer. As discussed below, this approximation leads to results consistent with oxygen vacancy calculations[29] and experimental measurements.[6]

A. First-principles calculations

The partial charge densities corresponding to the 2DEG calculated by integrating the occupied Ti states up to Fermi level are shown in Fig. 1. In the unrelaxed configuration, 2DEG is confined to within three unitcells of the surface and about 70% of the $0.4e$ charge resides in the top layer. Structural relaxation weaken the confinement through distortions of TiO_2 layer in which O planes move out of Ti planes. This results in the 2DEG spreading into about six layers as shown in Fig. 1(b). This distortion is 0.11 Å at the surface, but reduces gradually inside the slab and disappears completely below 6 layers. Since the 2DEG reside entirely in TiO_2 layers, distortions in SrO layers are quite small: only 0.03 Å at the surface. Hartree potential plotted in Fig. 1(c) and (d) show the variation of electrostatic potential felt by the electrons inside the slab. As the average curve shown in red indicate, the potential is relatively flat below 3-4 unitcells.

Fig. 1 suggests that the potential due to oxygen vacancies in STO result in 2DEG quite similar to that in a polar materials. In $KTaO_3$,[15] 2DEG is confined to 3 uc in unrelaxed structure and spreads to 7 uc upon relaxation. These observations are consistent with experimental measurements, that report similar subband structure in both systems[30]. However, note that the structural distortions at the $KTaO_3$ surface was 0.24 Å, which is twice as large as that of STO[15], possibly to counter the effect of polar catastrophe field.

The subband structures of the STO (001) slab are depicted in Fig. 2. In the unrelaxed structure, three pairs of bands cross Fermi level all having strong Ti-t_{2g} character from topmost layer. We denote the lowest band with d_{xy} character at Γ point by Γ_7'''[19], and the bands spin mixed by SOI by:

$$\Gamma_6'' = \begin{cases} d_{xz\downarrow} + id_{yz\downarrow} \\ d_{xz\uparrow} - id_{yz\uparrow} \end{cases} , \quad \Gamma_7'' = \begin{cases} d_{xz\downarrow} - id_{yz\downarrow} \\ d_{xz\uparrow} + id_{yz\uparrow} \end{cases} . \tag{1}$$

Degeneracy of t_{2g} states at Γ is broken in part by the surface potential that shifts Γ_7''' lower and by SOI which splits Γ'' bands by 2λ, where λ is the spin-orbit coupling parameter. For Ti in STO, from the energy gap we estimate $\lambda = 0.02$ eV, which is close to the atomic value of 23 meV[31]. In the relaxed structure, five d_{xy}-like bands from successive TiO_2 layers are occupied as shown in the right panel of Fig. 2, due to the spreading of 2DEG deeper upon relaxation. Lowest two bands are now of d_{xy} character from first and second layers, which is in good agreement with previous studies[30]. Experimental measurements[6] with a 2DEG density of $\sim 0.12e$ per surface unitcell reported the Fermi surfaces to be made of two concentric circles with light quasiparticle masses, which we can identify from Fig. 2 to be the two lowest Γ_7''' bands. Thus, we are able achieve the correct subband structure of electron rich STO surface with VCA calculations without complex vacancy calculations[29].

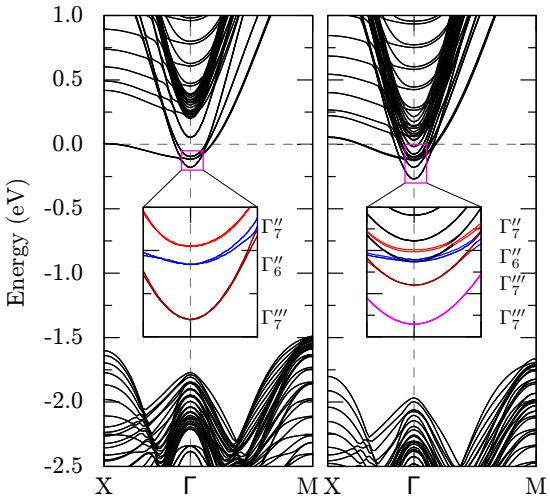

FIG. 2. (Color online) The electronic band structures with spin orbit coupling for $SrTiO_3$ slab with 0.4 electrons per surface unitcell in unrelaxed (left) and relaxed (right) structures. The inset shows a closer look at the 2DEG states. Band symmetries at Γ are marked right of the inset.

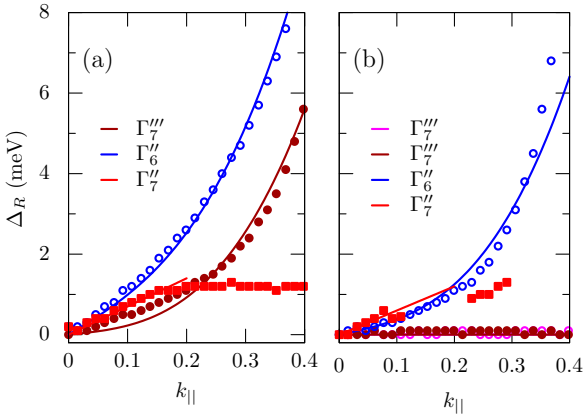

FIG. 3. (Color online) Spin splitting energy $\Delta_R = E_\uparrow - E_\downarrow$ for the 2DEG bands along the Γ-M/10 direction for the (a) unrelaxed and (b) relaxed structures from DFT calculations. The x-axis range correspond to the inset in Fig. 2. Solid lines are fits $\Delta_R = 2\alpha_{R1}k + 2\alpha_{R3}k^3$ and the fitting parameters are listed in Table. I.

The spin splitting, $\Delta_R = E_\uparrow - E_\downarrow$, calculated for the t_{2g} bands are plotted in Fig. 3. The colored lines correspond to bands with the same color in Fig. 2 and $k_{||}$ denotes k-path in the $\Gamma - M/10$ direction. Solid lines are fits using the equation $\Delta_R = 2\alpha_{R1}k + 2\alpha_{R3}k^3$, where α_R and α_{R3} denote linear and cubic Rashba parameters respectively. From results listed in Table. I, it can bee seen that cubic terms dominate Δ_R in Γ_6'' and Γ_7''' bands in the unrelaxed structure. The splitting in Γ_7'' is linear at small k and becomes nearly flat beyond 0.04 $Å^{-1}$, which is the typical behavior of linear Rashba splitting in d orbital systems[19]. Upon relaxation, spin splittings in Γ_7''' bands become substantially weaker upon relaxation.

Earlier theoretical models that reported cubic splitting in the middle d_{xz}/d_{yz}-like band (denoted as Γ_6'' in the present manuscript) are consistent with our findings[21,23]. However, we find the spin splitting in d_{xy} bands also to be cubic when nonzero. These results suggest that Rashba effect in STO is predominantly cubic. However, it is strongly orbital dependent and consequently sensitive to the location of the Fermi level. Structural relaxations are found to diminish Rashba effect in d_{xy} bands similar to polar systems such as $KTaO_3$[15]. To understand the results better, in the next section we construct a detailed tight-binding (TB) model for Ti-d and O-p states including upto next-nearest neighbor interactions.

TABLE I. Orbital characters, energies at Γ (in eV) and linear (α_{R1}/a in meV) and cubic (α_{R3}/a^3 in meV) Rashba pramaters obtained by fitting energy splitting in Fig. 3

Unrelaxed				Relaxed			
Orb	$E(\Gamma)$	α_{R1}/a	α_{R3}/a^3	Orb	$E(\Gamma)$	α_{R1}/a	α_{R3}/a^3
	-			$\Gamma_7'''(1)$	-0.27	0.0	0.0
Γ_7'''	-0.18	0.8	39.1	$\Gamma_7'''(2)$	-0.18	0.0	0.0
Γ_6''	-0.12	4.5	45.7	Γ_6''	-0.13	1.5	40.5
Γ_7''	-0.10	3.5	0.0	Γ_7''	-0.10	3.0	0.0

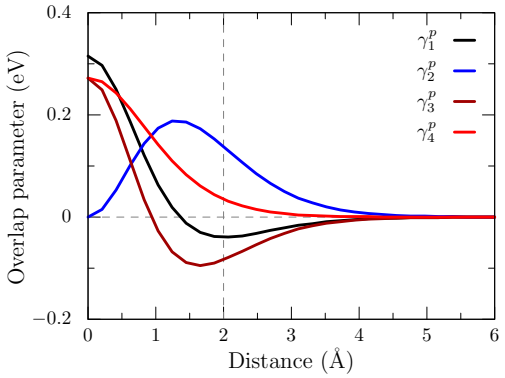

FIG. 4. (Color online) Electric field induced overlap parameters between Ti-d and O-p orbitals given in Eq. 2 with $\eta = 1$ eV/Å. Typical Ti-O bond lengths are ~ 2 Å.

B. Tight-binding model

To model the STO slab, we consider the surface TiO_2 layer that consists Ti atoms on a square lattice interconnected through O atoms. The Hamiltonian is represented in a 11 atomic orbital basis ($5d + 3p + 3p$). Matrix elements of the band structure part of the Hamiltonian can be derived in terms of Slater-Koster parameters[32]. To find the contribution of surface electric field, we numerically calculate the overlap between d and p orbitals at neighboring sites in the presence of an electric potential along z axis, $V = \eta z$. The radial part of wave functions are assumed to be Hydrogen-like with appropriate effective nuclear charges.[19] We find that there are four nonzero coupling parameters:

$$\gamma_1^p = \eta\langle d_{z^2}|z|p_z, \frac{a\hat{x}}{2}\rangle, \quad \gamma_2^p = \eta\langle d_{x^2-y^2}|z|p_z, \frac{a\hat{x}}{2}\rangle,$$
$$\gamma_3^p = \eta\langle d_{xz}|z|p_x, \frac{a\hat{x}}{2}\rangle, \quad \gamma_4^p = \eta\langle d_{yz}|z|p_y, \frac{a\hat{x}}{2}\rangle. \tag{2}$$

The orbital on the left of the inner product is at the origin and the right orbital is located on a neighboring atom at half the lattice parameter a, along the direction of the unit vector. Calculated parameters are plotted Fig. 4 as a function of Ti-O distance. Covalent radius of Ti-3d is around 1.3 Å, while that of O-2p is around 0.7 Å giving a typical Ti-O bond length of ~ 2 Å. In this range, strongest term is γ_2^p, and as shown below, it leads to effective coupling between $d_{x^2-y^2}$ and d_{xz}/d_{yz} orbitals, consistent with previous estimates.[19]

Since Ti-d and O-p are well separated in energy, the resulting 11×11 Hamiltonian matrix can be down-folded into an effective d orbital model with the help of quasi-degenerate perturbation theory[33]. In the basis $\{d_{z^2}, d_{x^2-y^2}, d_{xy}, d_{xz}, d_{yz}\}$, we get:

$$\mathcal{H}_d = \begin{pmatrix} h_1 & h_{12} & 0 & h_{14} & h_{15} \\ h_{12}^* & h_2 & 0 & h_{24} & h_{25} \\ 0 & 0 & h_3 & h_{34} & h_{35} \\ h_{14}^* & h_{24}^* & h_{34}^* & h_4 & 0 \\ h_{15}^* & h_{25}^* & h_{35}^* & 0 & h_5 \end{pmatrix}, \tag{3}$$

$$
\begin{aligned}
h_1 &= \varepsilon_0 + V_\sigma(\cos k_x + \cos k_y),\\
h_{12} &= \sqrt{3}V_\sigma(-\cos k_x + \cos k_y),\\
h_2 &= \varepsilon_1 + 3V_\sigma(\cos k_x + \cos k_y),\\
h_3 &= \varepsilon_2 + V_\pi(\cos k_x + \cos k_y),\\
h_4 &= \varepsilon_3 + V_\pi(\cos k_x),\\
h_5 &= \varepsilon_3 + V_\pi(\cos k_y),\\
h_{14} &= i\gamma_1 \sin k_x, \;\; h_{15} = i\gamma_1 \sin k_y,\\
h_{24} &= -i\gamma_2 \sin k_x, \;\; h_{25} = i\gamma_2 \sin k_y,\\
h_{34} &= i\gamma_3 \sin k_y, \;\; h_{35} = i\gamma_3 \sin k_x.
\end{aligned}
$$

with,

$$
\begin{aligned}
V_\sigma &= \frac{V_{pd\sigma}^2}{2(\varepsilon_p - \varepsilon_0)}, \;\; V_\pi = \frac{2V_{pd\pi}^2}{\varepsilon_p - \varepsilon_2}\\
\gamma_1 &= -\frac{(2\varepsilon_p - \varepsilon_0 - \varepsilon_2)(2\gamma_1^p V_{pd\pi} + \gamma_3^p V_{pd\sigma})}{4(\varepsilon_p - \varepsilon_0)(\varepsilon_p - \varepsilon_2)}\\
\gamma_2 &= -\frac{(2\varepsilon_p - \varepsilon_0 - \varepsilon_2)(2\gamma_2^p V_{pd\pi} - \sqrt{3}\gamma_3^p V_{pd\sigma})}{4(\varepsilon_p - \varepsilon_0)(\varepsilon_p - \varepsilon_2)}\\
\gamma_3 &= \frac{(2\varepsilon_p - \varepsilon_1 - \varepsilon_2)\gamma_4^p V_{pd\pi}}{2(\varepsilon_p - \varepsilon_1)(\varepsilon_p - \varepsilon_2)}
\end{aligned}
\tag{4}
$$

$$
\begin{aligned}
\alpha_1 &= -\frac{\sqrt{3}(2\varepsilon_p - \varepsilon_0 - \varepsilon_2)(2\gamma_1^p V_{pd\pi} + \gamma_3^p V_{pd\sigma})}{4(\varepsilon_p - \varepsilon_0)(\varepsilon_p - \varepsilon_2)(\varepsilon_0 - \varepsilon_3)}\\
\alpha_2 &= -\frac{(2\varepsilon_p - \varepsilon_0 - \varepsilon_2)(2\gamma_2^p V_{pd\pi} - \sqrt{3}\gamma_3^p V_{pd\sigma})}{4(\varepsilon_p - \varepsilon_0)(\varepsilon_p - \varepsilon_2)(\varepsilon_1 - \varepsilon_3)}\\
\alpha_3 &= \frac{(2\varepsilon_p - \varepsilon_1 - \varepsilon_2)\gamma_4^p V_{pd\pi}}{2(\varepsilon_p - \varepsilon_1)(\varepsilon_p - \varepsilon_2)(\varepsilon_2 - \varepsilon_3)}
\end{aligned}
$$

where, $\varepsilon_0, \varepsilon_1, \varepsilon_2, \varepsilon_3, \varepsilon_p$ are onsite energies and $V_{pd\sigma}$ and $V_{pd\pi}$ are the Slater-Koster overlap integrals between Ti-d and O-p orbitals. Note that the crystal momentum is defined to be $k_{x,y} \equiv k_{x,y}a$, so that it is dimensionless. Comparing the effective TB matrix in Eq. 3 with previously published model for d orbitals (sum of terms $\hat{T}_K$ and $\hat{T}_0$ from Ref. 19), we see that they are nearly identical except for the weak $V_{dd\delta}$ terms. Thus, oxygen states play no role in the Rasbha effect in the surface states of perovskite oxides and a model consisting only d orbitals is sufficient to capture the SOI effects these systems. However, since the strongest coupling is between d_{xz}/d_{yz} and $d_{x^2-y^2}$ orbitals, models incorporating only t_{2g} levels may be incomplete.

Finally, to incorporate the contribution of Ti-O-Ti bond distortions due to structural relaxation in the model, we construct the overlap parameters with oxygen atoms shifted along $+z$ direction by $\delta z = a\theta/2$, where θ is the angle made by Ti-O bond with the horizontal plane. We find that the resulting Hamiltonian is identical to Eq. 3 for small θ, except the parameters γ^p in Eq. 4 are replaced by

$$
\begin{aligned}
\gamma_1' &= \gamma_1^p + 2V_{pd\sigma}\theta - 4\sqrt{3}V_{pd\pi}\theta,\\
\gamma_2' &= \gamma_2^p - 2\sqrt{3}V_{pd\sigma}\theta + 4V_{pd\pi}\theta,\\
\gamma_3' &= \gamma_3^p - 4\sqrt{3}V_{pd\sigma}\theta + 4V_{pd\pi}\theta,\\
\gamma_4' &= \gamma_4^p - 4V_{pd\pi}\theta.
\end{aligned}
\tag{5}
$$

Clearly, $\gamma' \to \gamma^p$ as $\theta \to 0$. Since, typically $V_{pd\sigma} \leq 0$ and $V_{pd\pi} > 0$, lattice distortions counteract the effect of surface potential and weaken the field induced Ti-O coupling parameters consistent with our DFT calculations depicted in Fig. 2.

1. *Rashba Hamiltonian*

The Löwding downfolding procedure can be applied on the model in Eq. 3 to derive effective 2×2 Hamiltonians for individual bands around Γ point, provided that coupling between the bands are weaker than the energy separating

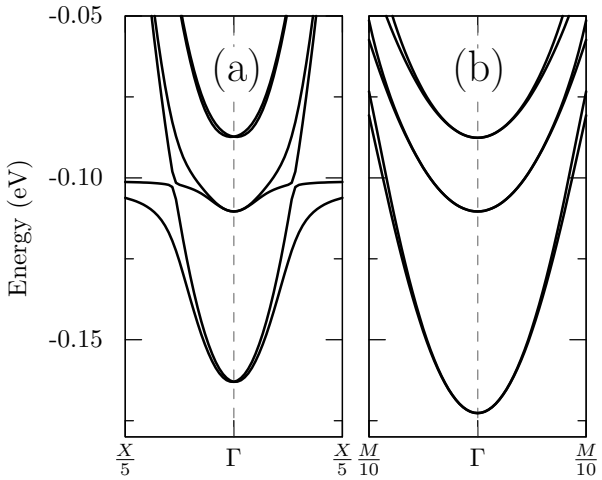

FIG. 5. Tight-binding band structures showing Rashba splitting in Ti-t_{2g} bands. (a) Nearest neighbor model with $\gamma = \{0, 0, 0.03\}$ eV and (b) next-nearest neighbor model with $\gamma = \{0, 0, 0.6\}$ eV and $\gamma^n = \{0, 0, -0.6\}$ eV. Other parameters in the model obtained from fitting to the DFT band structure are (in eV), $\varepsilon_0 = 1.5, \varepsilon_1 = 2, \varepsilon_2 = -0.11, \varepsilon_3 = -0.05, V_\sigma = -0.2, V_\pi = -1, V_{d\sigma} = -0.02, V_{d\pi} = -0.025$ and $\lambda = 0.02$.

them; i.e., $\alpha, V_\sigma, V_\pi \ll \lambda \ll \varepsilon$. Using, $\alpha_1 = \sqrt{3}\gamma_1/(\varepsilon_0 - \varepsilon_3), \alpha_2 = \gamma_2/(\varepsilon_1 - \varepsilon_3)$ and $\alpha_3 = \gamma_3/(\varepsilon_2 - \varepsilon_3)$ for simplicity and retaining terms linear in α, λ and up to cubic in k, we get:

$$
\begin{aligned}
\mathcal{H}(\Gamma_7''') &= (\varepsilon_2 - \frac{V_\pi}{2}k^2)\mathbb{1} - \alpha_3\lambda(k_y\sigma_x - k_x\sigma_y) + \frac{\alpha_3\lambda}{6}(k_y^3\sigma_x - k_x^3\sigma_y), \\
\mathcal{H}(\Gamma_6'') &= (\varepsilon_3 - \frac{\lambda}{2} - \frac{V_\pi}{4}k^2)\mathbb{1} + \alpha_1\lambda(k_y\sigma_x - k_x\sigma_y) - \frac{V_\pi}{4}(\alpha_1 + \alpha_2 - \alpha_3)(k_y\sigma_x + k_x\sigma_y)(k_x^2 - k_y^2), \\
\mathcal{H}(\Gamma_7'') &= (\varepsilon_3 + \frac{\lambda}{2} - \frac{V_\pi}{4}k^2)\mathbb{1} + (\alpha_2 + \alpha_3)\lambda(k_y\sigma_x - k_x\sigma_y) \\
&\quad + \frac{V_\pi}{4}(\alpha_1 + \alpha_2)(k_y\sigma_x + k_x\sigma_y)(k_x^2 - k_y^2) - \frac{\lambda}{6}(\alpha_2 + \alpha_3)(k_y^3\sigma_x - k_x^3\sigma_y),
\end{aligned} \tag{6}
$$

Consistent with previous calculations, we find that all bands have linear Rashba terms in the Hamiltonian[19,21]. However, in the bands Γ_6'' and Γ_7'' it is possible to have dominant cubic-k splitting when linear terms are suppressed by $\alpha_1 = 0$ and $\alpha_2 = \alpha_3 = 0$ respectively. In Eq. 6 one can see that spin splitting in the relaxed structure shown in Fig. 3(b) can be explained qualitatively by $\gamma = \{0, \gamma_2, 0\}$, which leads to zero splitting in Γ_7''', cubic in Γ_6'' and linear in Γ_7''. However, we must not take Eq. 6 too seriously since the assumption $V_\sigma, V_\pi \ll \lambda$ is not valid in STO as discussed below. In such cases, the Hamiltonian for Γ_6'' and Γ_7'' cannot be separated and one has to work with a 4×4 matrix[15].

It appears that cubic-k splitting of Γ_7''' band in the unrelaxed structure shown in Fig. 3(a) is not consistent with the 2×2 Hamiltonian in Eq. 6 since the same parameter α_3 is responsible for both linear and cubic terms. This is because, expressions in Eq. 6 are valid only for small k, and coupling between Γ_7''' and Γ_6'' leads to the splitting as can be seen from Fig. 2. Diagonalizing the full Hamiltonian, which retains this interaction, we find the energy splitting:

$$
\Delta E(\Gamma_7''') = -2\alpha_3\lambda k + \frac{\alpha_3\lambda}{3}\left(1 - \frac{3V_\pi}{\varepsilon_2 - \varepsilon_3}\right)(k_x^3 + k_y^3) \tag{7}
$$

Fitting the TB model with the DFT electronic structure, we find that V_π is ~ -1 eV, whereas $\varepsilon_2 - \varepsilon_3 \sim 0.06$, $\lambda = 0.02$ and $\gamma_3 = 0.03$ (all units in eV). Substituting in Eq. 7, we get $\Delta E(\Gamma_7''') = -0.02k + 0.17(k_x^3 + k_y^3)$, which has cubic-$k$ term much stronger, which explains the spin-splitting in the unrelaxed band structure. In Fig. 5(a) we show the TB model with $\gamma_3 = 0.03$ eV which is in good agreement with the spin-splitting in DFT bands of the unrelaxed STO. A more accurate fit to the DFT bands suggest parameters $\gamma = \{0, 0.3, 0.02\}$ for the unrelaxed structure and $\gamma = \{0, 0.3, 0\}$ for the relaxed structure. Thus, structural relaxation diminishes field induced coupling γ_3, while γ_2 is unaffected.

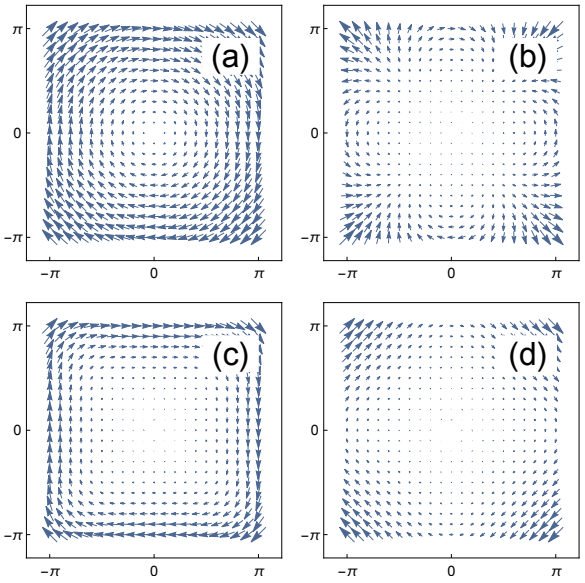

FIG. 6. Pseudospin distribution in the 2D Brillouin zone arising from the 2×2 Hamiltonians (a) $H_{R1} = (k_y\sigma_x - k_x\sigma_y)$, (b) $H_{R3} = (k_y\sigma_x - k_x\sigma_y)^3$, (c) $H_{R4} = (k_y^3\sigma_x - k_x^3\sigma_y)$ and (d) $H_{R5} = (k_y^3\sigma_x - k_x^3\sigma_y) + 3k_xk_y(k_x\sigma_x - k_y\sigma_y)$.

C. Contribution from next-nearest neighbors

To incorporate the effect of diagonal neighbors at $(\pm a, \pm a, 0)$ on the dispersion of Ti-d bands, we calculate matrix elements between these orbitals:

$$H_{nn} = \begin{pmatrix} h_1 & 0 & h_3 & \gamma_1^n h_4 & \gamma_1^n h_5 \\ 0 & 2h_2 & 0 & \gamma_2^n h_4 & -\gamma_2^n h_5 \\ h_3^* & 0 & 3h_1 & \gamma_3^d h_5 & \gamma_3^n h_4 \\ \gamma_1^n h_4^* & \gamma_2^n h_4^* & \gamma_3^n h_5^* & h_2 & h_6 \\ \gamma_1^n h_5^* & -\gamma_2^n h_5^* & \gamma_3^n h_4^* & h_6^* & h_2 \end{pmatrix} \tag{8}$$

$$h_1 = V_{d\sigma}\cos k_x \cos k_y, \quad h_2 = V_{d\pi}\cos k_x \cos k_y,$$
$$h_3 = \sqrt{3}V_{d\sigma}\sin k_x \sin k_y, \quad h_4 = -i\cos k_y \sin k_x,$$
$$h_5 = i\cos k_x \sin k_y, \quad h_6 = -2V_{d\pi}\sin k_x \sin k_y.$$

where, $V_{d\sigma}, V_{d\pi}, \gamma_1^n, \gamma_2^n$ and γ_3^n are the new direct d orbital overlap parameters. Notice that matrix elements have products of k_x and k_y terms unlike the nearest neighbor model which contain sum of these terms. To see if this affects Rashba splitting, we downfold the Hamiltonian as before and find the matrix element coupling spin-up and spin-down states of Γ_7''' to be:

$$\begin{aligned} \mathcal{H}_{12}(\Gamma_7''') = &- \alpha_3^n\lambda(ik_x + k_y) \\ &+ \frac{\alpha_3^n\lambda}{6}(ik_x^3 + 3k_x^2k_y + 3ik_xk_y^2 + k_y^3) \end{aligned} \tag{9}$$

The next-nearest neighbor coupling also leads to both linear and cubic terms. However, while the linear part is identical to the nearest neighbor model, the cubic part has additional terms, which suggest that if the parameters are such that $\alpha_3^n = -\alpha_3$, the linear part can cancel out leaving a partial cubic part. This is confirmed by the band structure plot in Fig. 5(b) which shows cubic splitting in all bands with a model containing both nearest and next-nearest neighbor interactions.

Finally, we note that cubic terms in the Rashba Hamiltonians in Eq. 6 and Eq. 7 are different from the model for cubic Rashba from $k \cdot p$ theory discussed in introduction. For example, cubic terms for Γ_7''' band from nearest neighbor model is $(ik_x^3 + k_y^3)$ and $(ik_x^3 + 3ik_xk_y^2 + 3k_x^2k_y + k_y^3)$ from next-nearest neighbor model. These are different from the cubic term from H_{R3}, which is $(-ik_x^3 + 3ik_xk_y^2 - 3k_x^2k_y + k_y^3)$. These affect the rotation of pseudospins in reciprocal space, and consequently width of the WAL spectra[9]. We have plotted in Fig. 6 pseudospin distribution in

the 2D Brillouin zone for various 2×2 Rashba Hamiltonians discussed in this paper. For the linear Rashba $\mathcal{H}_{R1}$, the pseudospin rotates 2π for one revolution in k space while the cubic Rashba Hamiltonian $\mathcal{H}_{R3}$ rotates 6π for a similar revolution. Surprisingly, the pseudospin distributions from cubic Hamiltonians from nearest neighbor model (H_{R4}) and next-nearest neighbor (H_{R5}) resemble H_{R3} in magnitude, but resemble H_{R1} in rotation. The significance of these results in the context of spin-relaxation measurements needs to be investigated further.

IV. CONCLUSIONS

Spin-orbit coupling effects in the 2DEG at (001) surface of $SrTiO_3$ is studied with the help of first principles calculations and tight-binding models. Consistent with experimental measurements, lowest bands occupied by 2DEG are found to be of d_{xy} character originating from the first and second layers. Spin splitting in Γ_6'' is predominantly cubic and is unaffected by structural relaxation at the surface. Cubic spin splitting in d_{xy} arises from its coupling with the heavy electron Γ_6'' band, which is suppressed by structural relaxation. With the help of a tight-binding model Hamiltonian, we show that effect of O-p states can be incorporated via effective d orbital overlap parameters. The surface electric field induces new overlap parameters between Ti-d and O-p that lead to spin splitting in the presence of spin-orbit coupling. The model is fit to DFT band structure and is shown to reproduce the cubic-k splitting well. However, eigenfunctions of the cubic part of the Hamiltonian is found to be different from the standard cubic Rashba model.

V. ACKNOWLEDGMENTS

This research was supported by the US Department of Energy, Basic Energy Sciences, Office of Science, Materials Sciences and Engineering Division.

---

* kavungalvees@ornl.gov

[1] C. Cen, S. Thiel, J. Mannhart, and J. Levy, "Oxide nanoelectronics on demand," Science **323**, 1026 (2009).

[2] C. He, T. D. Sanders, M. T. Gray, F. J. Wong, V. V. Mehta, and Y. Suzuki, "Metal-insulator transitions in epitaxial $LaVO_3$ and $LaTiO_3$ films," Phys. Rev. B **86**, 081401 (2012).

[3] A. Ohtomo and H. Y. Hwang, "A high-mobility electron gas at the $LaAlO_3/SrTiO_3$ heterointerface," Nature **427**, 423 (2004).

[4] N. Reyren, S. Thiel, A. D. Caviglia, L. F. Kourkoutis, G. Hammerl, C. Richter, C. W. Schneider, T. Kopp, A.-S. Ruetschi, D. Jaccard, and et al., "Superconducting interfaces between insulating oxides," Science **317**, 11961199 (2007).

[5] A. Brinkman, M. Huijben, M. van Zalk, J. Huijben, U. Zeitler, J. C. Maan, W. G. van der Wiel, G. Rijnders, D. H. A. Blank, and H. Hilgenkamp, "Magnetic effects at the interface between non-magnetic oxides," Nature Materials **6**, 493 (2007).

[6] W. Meevasana, P. D. C. King, R. H. He, S-K. Mo, M. Hashimoto, A. Tamai, P. Songsiriritthigul, F. Baumberger, and Z-X. Shen, "Creation and control of a two-dimensional electron liquid at the bare $SrTiO_3$ surface," Nature Materials **10**, 114 (2011).

[7] A. F. Santander-Syro, O. Copie, T. Kondo, F. Fortuna, S. Pailhs, R. Weht, X. G. Qiu, F. Bertran, A. Nicolaou, A. Taleb-Ibrahimi, and et al., "Two-dimensional electron gas with universal subbands at the surface of $SrTiO_3$," Nature **469**, 189 (2011).

[8] S. McKeown Walker, A. de la Torre, F. Y. Bruno, A. Tamai, T. K. Kim, M. Hoesch, M. Shi, M. S. Bahramy, P. D. C. King, and F. Baumberger, "Control of a two-dimensional electron gas on $SrTiO_3$(111) by atomic oxygen," Phys. Rev. Lett. **113**, 177601 (2014).

[9] H. Nakamura, T. Koga, and T. Kimura, "Experimental evidence of cubic rashba effect in an inversion-symmetric oxide," Phys. Rev. Lett. **108**, 206601 (2012).

[10] Y. A. Bychkov and E. I. Rashba, "Oscillatory effects and the magnetic susceptibility of carriers in inversion layers," J. Phys. C **17**, 6039 (1984).

[11] J. Nitta, T. Akazaki, H. Takayanagi, and T. Enoki, "Gate control of spin-orbit interaction in an inverted $In_{0.53}Ga_{0.47}As/In_{0.52}Al_{0.48}As$ heterostructure," Phys. Rev. Lett. **78**, 1335 (1997).

[12] R. Winkler, "Rashba spin splitting in two-dimensional electron and hole systems," Phys. Rev. B **62**, 4245–4248 (2000).

[13] J. B. Miller, D. M. Zumbühl, C. M. Marcus, Y. B. Lyanda-Geller, D. Goldhaber-Gordon, K. Campman, and A. C. Gossard, "Gate-controlled spin-orbit quantum interference effects in lateral transport," Phys. Rev. Lett. **90**, 076807 (2003).

[14] A. D. Caviglia, M. Gabay, S. Gariglio, N. Reyren, C. Cancellieri, and J.-M. Triscone, "Tunable rashba spin-orbit interaction at oxide interfaces," Phys. Rev. Lett. **104**, 126803 (2010).

[15] K. V. Shanavas and S. Satpathy, "Electric field tuning of the rashba effect in the polar perovskite structures," Phys. Rev. Lett. **112**, 086802 (2014).

[16] G. M. Minkov, A. A. Sherstobitov, A. V. Germanenko, O. E. Rut, V. A. Larionova, and B. N. Zvonkov, "Antilocalization and spin-orbit coupling in the hole gas in strained GaAs/$In_xGa_{1-x}As$/GaAs quantum well heterostructures," Phys. Rev. B **71**, 165312 (2005).

[17] R. Winkler, D. Culcer, S. J. Papadakis, B. Habib, and M. Shayegan, "Spin orientation of holes in quantum wells," Semicond. Sci. Tech. **23**, 114017 (2008).

[18] R. Moriya, K. Sawano, Y. Hoshi, S. Masubuchi, Y. Shiraki, A. Wild, C. Neumann, G. Abstreiter, D. Bougeard, T. Koga, and T. Machida, "Cubic rashba spin-orbit interaction of a two-dimensional hole gas in a strained-Ge/SiGe quantum well," Phys. Rev. Lett. **113**, 086601 (2014).

[19] K. V. Shanavas, Z. S. Popović, and S. Satpathy, "Theoretical model for rashba spin-orbit interaction in d electrons," Phys. Rev. B **90**, 165108 (2014).

[20] K. V. Shanavas, "Overview of theoretical studies of rashba effect in polar perovskite surfaces," J. Electron Spectrosc. **201**, 121 (2015).

[21] Z. Zhong, A. Tóth, and Karsten Held, "Theory of spin-orbit coupling at $LaAlO_3/SrTiO_3$ interfaces and $SrTiO_3$ surfaces," Phys. Rev. B **87**, 161102 (2013).

[22] G. Khalsa, B. Lee, and A. H. MacDonald, "Theory of t_{2g} electron-gas rashba interactions," Phys. Rev. B **88**, 041302 (2013).

[23] Y. Kim, R. M. Lutchyn, and C. Nayak, "Origin and transport signatures of spin-orbit interactions in one- and two-dimensional $SrTiO_3$ -based heterostructures," Phys. Rev. B **87**, 245121 (2013).

[24] G. Kresse and J. Hafner, "Ab-initio molecular dynamics for liquid metals," Phys. Rev. B **47**, 558 (1993); G. Kresse and J. Furthmüller, "Efficient iterative schemes for *ab initio* total-energy calculations using a plane-wave basis set," *ibid.* **54**, 11169 (1996).

[25] P. E. Blöchl, "Projector augmented-wave method," Phys. Rev. B **50**, 17953 (1994).

[26] K. V. Shanavas and D. J. Singh, "Doping $SrTiO_3$ supported FeSe by excess atoms and oxygen vacancies," (2015).

[27] K. V. Shanavas and S. Satpathy, "Effective tight-binding model for MX_2 under electric and magnetic fields," Phys. Rev. B **91**, 235145 (2015).

[28] Z. S. Popović, S. Satpathy, and R. M. Martin, "Origin of the two-dimensional electron gas carrier density at the $LaAlO_3$ on $SrTiO_3$ interface," Phys. Rev. Lett. **101**, 256801 (2008).

[29] J. Shen, H. Lee, R. Valentí, and H. O. Jeschke, "*Ab initio* study of the two-dimensional metallic state at the surface of $SrTiO_3$: Importance of oxygen vacancies," Phys. Rev. B **86**, 195119 (2012).

[30] P. D. C. King, R. C. Hatch, M. Bianchi, R. Ovsyannikov, C. Lupulescu, G. Landolt, B. Slomski, J. H. Dil, D. Guan, J. L. Mi, E. D. L. Rienks, J. Fink, A. Lindblad, S. Svensson, S. Bao, G. Balakrishnan, B. B. Iversen, J. Osterwalder, W. Eberhardt, F. Baumberger, and Ph. Hofmann, "Large tunable rashba spin splitting of a two-dimensional electron gas in Bi_2Se_3," Phys. Rev. Lett. **107**, 096802 (2011).

[31] F. Herman and S. Skillman, *Atomic Structure Calculations* (Prentice-Hall, New Jersey, 1963).

[32] J. C. Slater and G. F. Koster, "Simplified LCAO method for the periodic potential problem," Phys. Rev. **94**, 1498 (1954).

[33] P.-O. Löwdin, "A note on the quantum-mechanical perturbation theory," J. Chem. Phys. **19**, 1396 (1951).